Escherichia coli SPFH membrane microdomain proteins HflKC contribute to aminoglycoside and oxidative stress tolerance

Aimee K. WESSEL[1†], Yutaka YOSHII[1†], Alexander REDER[2], Rym BOUDJEMAA[3], Magdalena SZCZESNA[1,6], Jean-Michel BETTON[4], Joaquin BERNAL-BAYARD[1,7], Christophe BELOIN[1], Daniel LOPEZ[5], Uwe VÖLKER[2], Jean-Marc GHIGO[1*]

[1] *Institut Pasteur, Université de Paris-Cité, CNRS UMR6047, Genetics of Biofilms Laboratory F-75015 Paris, France.*

[2] *Department of Functional Genomics, Interfaculty Institute for Genetics and Functional Genomics, University Medicine Greifswald, 17487 Greifswald, Germany.*

3 Abbelight, 191 avenue Aristide Briand, 94230 Cachan

[4] *Institut Pasteur, Université de Paris-Cité, UMR UMR6047, Stress adaptation and metabolism in enterobacteria 75015 Paris, France.*

[5] *Universidad Autonoma de Madrid, Centro Nacional de Biotecnologia, Campus de Cantoblanco, Calle Darwin 3, 28049 Madrid, España*

[6] *Centre for Bacteriology Resistance Biology, Imperial College London, London, SW7 2AZ,UK*

[7] *Departamento de Genética, Facultad de Biología, Universidad de Sevilla, Apartado 1095, 41080 Sevilla, Spain*

† AW and YY equally contributed to this work. Author order was determined both alphabetically and in order of increasing seniority.

[*]**Corresponding author:** Jean-Marc Ghigo (jean-marc.ghigo@pasteur.fr)

Running Title: *E. coli* SPFH proteins contribute to stress tolerance

Keywords

Membrane microdomains; SPFH proteins; Flotillin; Lipid raft; Stress tolerance; *Escherichia coli*

ABSTRACT

Many eukaryotic membrane-dependent functions are often spatially and temporally regulated by membrane microdomains (FMMs) also known as lipid rafts. These domains are enriched in polyisoprenoid lipids and scaffolding proteins belonging to the Stomatin, Prohibitin, Flotillin, and HflK/C (SPFH) protein superfamily that was also identified in Gram-positive bacteria. By contrast, little is still known about FMMs in Gram-negative bacteria. In *Escherichia coli* K12, 4 SPFH proteins, YqiK, QmcA, HflK, and HflC, were shown to localize in discrete polar or lateral inner-membrane locations, raising the possibility that *E. coli* SPFH proteins could contribute to the assembly of inner-membrane FMMs and the regulation of cellular processes.

Here we studied the determinant of the localization of QmcA and HflC and showed that FMM-associated cardiolipin lipid biosynthesis is required for their native localization pattern. Using Biolog phenotypic arrays, we showed that a mutant lacking all SPFH genes displayed increased sensitivity to aminoglycosides and oxidative stress that is due to the absence of HflKC. Our study therefore provides further insights into the contribution of SPFH proteins to stress tolerance in *E. coli*.

IMPORTANCE

Eukaryotic cells often segregate physiological processes in cholesterol-rich functional membrane micro-domains. These domains are also called lipid rafts and contain proteins of the Stomatin, Prohibitin, Flotillin, and HflK/C (SPFH) superfamily, which are also present in prokaryotes but were mostly studied in Gram-positive bacteria. Here, we showed that the cell localization of the SPFH proteins QmcA and HflKC in the Gram-negative bacteria *E. coli* is altered in absence of cardiolipin lipid synthesis. This suggests that cardiolipins contribute to *E. coli* membrane microdomain assembly. Using a broad phenotypic analysis, we also showed that HflKC contribute to *E. coli* tolerance to aminoglycosides and oxidative stress. Our study, therefore, provides new insights into the cellular processes associated with SPFH proteins in *E. coli*.

71 **INTRODUCTION**

72

73 In addition to separating the intracellular content of cells from the environment, lipid
74 bilayer membranes also contribute to specialized functions, including cross-membrane
75 transport, enzymatic activity, signaling as well as anchoring of cytoskeletal and
76 extracellular structures (1, 2). In eukaryotes, these membrane-dependent functions are
77 often spatially and temporally regulated by functional membrane microdomains (FMMs)
78 called lipid rafts (3-5). FMMs compartmentalize membrane cellular processes in
79 cholesterol- and sphingolipid-enriched membrane regions formed upon lipid-lipid, lipid-
80 protein and protein-protein interactions (5-7). A family of membrane proteins called
81 SPFH proteins (for Stomatin/Prohibitin/Flotillin/HflK/C) has been shown to localize in
82 eukaryotic lipid rafts and to recruit and provide a stabilizing scaffold to other raft-
83 associated proteins (8-13).

84

85 Whereas most prokaryotes lack sphingolipids and cholesterol (14), the Gram-positive
86 bacteria *Bacillus subtilis* and *Staphylococcus aureus* can also compartmentalize cellular
87 processes in functional membrane microdomains (FMMs) (14-16). Although whether
88 bacterial FMMs display a distinct lipidic composition needs to be more firmly established,
89 they have been reported to be enriched in polyisoprenoid lipids as well as in cardiolipins
90 at the cell poles (14-19)

91

92 FMMs also contain SPFH proteins, including flotillins, and a pool of proteins involved
93 in diverse cellular processes (14, 16). In *B. subtilis*, flotillins FloT and FloA colocalize in
94 membrane foci and contribute to the assembly of membrane protein complexes (20-23).
95 Lack of flotillins impairs biofilm formation, sporulation, protease secretion, motility, and
96 natural competence, indicating that the formation of FMMs also plays critical cellular
97 roles in *B. subtilis* (15, 20, 24-27).
98 SPFH proteins are also present in Gram-negative bacteria, and *Escherichia coli* K12 even
99 possesses four genes, *yqiK*, *qmcA*, *hflK*, and *hflC*, which encode proteins with an SPFH
100 domain and a N-terminal transmembrane segment (28). QmcA and YqiK are predicted to
101 face the cytoplasmic compartment, while HflK and HflC are predicted to be exposed in
102 the periplasm, forming the HflKC complex negatively regulating the protease activity of

103 FtsH against membrane proteins (29-32). HflC and QmcA are detected in *E. coli*
104 membrane fractions resistant to solubilization by non-ionic detergents (detergent-resistant
105 membranes or DRM) that are often used as - debatable - proxies for FMMs (33-36).
106 Fluorescent microscopy also showed that *E. coli* SPFH proteins HflC and QmcA are
107 localized in discrete polar or lateral membrane foci (37), raising the possibility that *E. coli*
108 SPFH proteins could localize in inner-membrane FMMs and regulate specific cellular
109 processes (38). However, apart from the functional and structural description of HflKC
110 as a regulator of the FtsH membrane protease (29, 32, 39) and a recent study suggesting
111 that YqiK is involved in cell motility and resistance to ampicillin (40), the functions of
112 FMM in *E. coli* and other Gram-negative bacteria are still poorly understood.
113 In this study, we used fluorescent and super-resolution microscopy to perform a detailed
114 analysis of QmcA and HflC membrane localization signals. We then showed that the
115 integrity of QmcA and HflC protein domains is required for their inner membrane
116 localization, and that the lack of cardiolipin and isoprenoid lipids known to associate with
117 FMMs alters their localization. Moreover, using single and multiple SPFH gene mutants,
118 we showed that HflKC SPFH proteins contribute to aminoglycosides and oxidative stress
119 resistance. Our study therefore provides new insights into the determinants of cellular
120 localization and the function associated with *E. coli* SPFH proteins.

121 **RESULTS**
122
123 **Chromosomal *E. coli* SPFH fluorescent fusion proteins show distinct localization**
124 **patterns.**
125
126 To investigate the determinant of cell localization of *E. coli* SPFH proteins, we first
127 tagged YqiK and QmcA, which C-termini are predicted to be in the cytoplasm (31), with
128 a C-terminal monomeric super folder green fluorescent protein (msfGFP). We then
129 tagged HflC and HflK, which C-termini are predicted to be in the periplasm (31), with
130 the C-terminal monomeric red fluorescent protein mCherry. All these fusions were
131 expressed under their own promoter from their native chromosomal location (Sup. Fig.
132 S1). Epifluorescence and super-resolution microscopy confirmed the previously reported
133 polar localization of HflK and HflC (37) (Fig. 1 and Sup. Fig. S2), with 94% and 91%
134 polar localization pattern for HflC-mCherry and HflK-mCherry, respectively (n=150). By
135 contrast, C-terminally tagged QmcA-GFP showed punctate foci distributed throughout
136 the cell body, with 96% of the cells harboring 5 foci or more (n=150) (Fig. 1CD).
137 However, we could not detect YqiK-GFP, possibly due to its low native chromosomal
138 expression level. We then used anti-GFP or mCherry antibodies to perform
139 immunodetection on cytoplasmic as well as inner and outer membrane fractions of *E. coli*
140 strains expressing either HflC-mCherry or QmcA-GFP. In agreement with previous
141 results (31, 38), both fusion proteins were detected in the inner membrane fraction (Fig.
142 2).
143
144 **Domain swap analysis shows that protein integrity is essential for QmcA-GFP and**
145 **HflC-mCherry localization.**
146
147 To identify HflC and QmcA membrane localization signals, we constructed multiple
148 fluorescently tagged truncated versions of both proteins. We tagged with msfGFP a
149 QmcA protein reduced to its transmembrane region and SPFH domain (TM^{QmcA}-
150 $SPFH^{QmcA}$-GFP) and, separately, one reduced to the QmcA transmembrane region only
151 (TM^{QmcA}-GFP) (Fig. 3A). To test the role of the QmcA transmembrane region, we also
152 swapped TM^{QmcA} in the three constructs by the single-spanning TM domain of the phage
153 coat protein Pf3 (TM^{Pf3}), which orients subsequent amino acids to the cytosol (38) (Fig.
154 3A). Similarly, in addition to the full length HflC-mCherry, we tagged with mCherry the
155 HflC transmembrane region and SPFH domain (TM^{HflC}-$SPFH^{HflC}$-mCherry) and,

156 separately, only its TM region (TM^{HflC}-mCherry) (Fig. 3B). We also swapped the HflC
157 TM region with the single-spanning TM region of colistin M immunity protein (TM^{Cmi}),
158 which orients subsequent amino acids to the periplasm (39) (Fig. 3B). Epifluorescence
159 microscopy of HflC and QmcA derivative fusions showed that in addition to full-length
160 constructs only full-length constructs with swapped TM (TM^{Pf3}-QmcA-GFP and TM^{Cmi}-
161 HflC-mCherry) displayed significant punctate foci or polar localization, respectively (Fig.
162 3AB), although at reduced frequency compared to native QmcA-GFP and HflC-mCherry.
163 Finally, we prepared inner and outer membrane fractions of *E. coli* strains expressing
164 each QmcA and HflC derivative, and we observed that all these constructs were still
165 mainly located in the inner membrane fraction. This indicates that, while we observed
166 that QmcA-GFP and HflC-mChery derivatives exhibit altered cell localization, they do
167 not exhibit significant mis-localization and remain located in the inner membrane (Sup.
168 Fig. S3). These results therefore indicated that specific QmcA and HflC localization
169 requires the combination of a transmembrane and full cytoplasmic (QmcA) or
170 periplasmic (HflC) domain.
171
172 **Lack of cardiolipin and isoprenoid lipid synthesis alters the cell localization of**
173 **QmcA and HflC.**
174
175 FMMs were proposed to be enriched with negatively charged cardiolipins and
176 isoprenoids, which promote the localization of polar proteins and modulation of
177 membrane lipid fluidity (15, 17, 18, 24, 41-44). We first tested whether alteration of
178 cardiolipin synthesis could cause mis-localization of *E. coli* SPFH proteins QmcA or
179 HflKC in a mutant lacking the major cardiolipin synthases *clsABC* (45). Whereas super-
180 resolution microscopy analysis only showed an alteration of the number of QmcA-GFP
181 punctates (1-5 cluster per bacterium) compared to WT (10-15 cluster per bacterium) (Fig.
182 4A and Sup. Fig. S4), the localization of HflC-mCherry showed a drastic loss of polar
183 localization pattern (Fig. 4B and Supp. Fig. S4). We then used an *idi* mutant with reduced
184 isoprenoid lipid synthesis due to the lack of isomerization of isopentenyl diphosphate
185 (IPP) into dimethylallyl diphosphate (DMAPP) (46, 47). Whereas QmcA-GFP punctate
186 localization was not affected, HflC-mCherry polar localization was not abolished in the
187 Δ*idi* mutant (Fig. 4A and Sup. Fig. S4). These results demonstrated that the alteration of
188 cardiolipin and, in a lesser extent, isoprenoid lipid synthesis pathway affects HflC fusion
189 protein localization in *E. coli*.

190
191 **Phenotypic analysis of *E. coli* SPFH mutant shows that only the absence of HflKC**
192 **increases *E. coli* sensitivity to aminoglycosides and oxidative stress.**
193
194 To identify potential phenotypes and functions associated with the *E. coli* SPFH proteins
195 YqiK, QmcA, HflK and HflC, we introduced single and multiple deletions of the
196 corresponding SPFH genes. We observed that neither single mutants nor the quadruple
197 Δ*hflK,* Δ*hflC,* Δ*qmcA*, and Δ*yqiK* (hereafter referred to Δ*SPFH* mutant) displayed any
198 significant growth defects in rich or minimal media (Fig. 5A and Sup. Fig. S5A).
199 Considering the role of SPFH proteins in the activation of inner-membrane kinases
200 involved in *B. subtilis* biofilm formation (15), we tested adhesion and biofilm capacity of
201 WT and ΔSPFH strains but could not detect any significant differences between these two
202 strains. We then used Biolog™ phenotypic microarrays to perform a large-scale
203 phenotypic assay comparing an *E. coli* WT and Δ*SPFH* mutant (Sup. Table S1). This
204 analysis revealed that the Δ*SPFH* mutant is metabolically less active when grown in the
205 presence of various aminoglycosides (tobramycin, capreomycin, sisomicin and
206 paromomycin) or when exposed to paraquat (Fig. 5B and Sup. Fig. S5BC). Consistently,
207 the minimal inhibitory concentration (MIC) for tobramycin of the Δ*SPFH* mutant was 3-
208 fold lower than that of the WT MIC (Fig.5C), and the sensitivity of the Δ*SPFH* mutant to
209 paraquat was increased compared to the WT (Fig. 5D and Sup. Fig. S5D). Test of
210 individual SPFH-gene mutants for their sensitivity to tobramycin and paraquat showed
211 that the HflKC complex is the sole responsible for both phenotypes, as both single *hflK*
212 and *hflC* or a double *hflKC* mutants displayed increased sensitivity to tobramycin and
213 oxidative stress (Fig. 5CD and Sup. Fig. S5E). This phenotype could be complemented
214 upon the introduction of a plasmid expressing *hflKC* genes in the double *hflKC* mutant
215 (Sup. Fig. S6). Of note, C-terminally tagged HflC-mCherry and HflK-mCherry displayed
216 wildtype MIC for tobramycin and paraquat, indicating that both fusions were functional
217 and relevant proxies for the bacterial localization of the HflKC complex (Sup. Fig. S6).
218
219

220 **Contribution of HflC localization to tobramycin and paraquat tolerance**

221

222 Whereas an Δ*idi* mutant showed no significant difference compared to the WT, the MIC
223 for tobramycin and paraquat of a Δ*clsABC* mutant was reduced by 2 to 3-fold, which is
224 consistent with the respective impact of a *cls* and *idi* mutation on HflC localization (Fig.
225 4BD and Fig.5CD). Considering the scaffolding role of HflKC and the importance of cell
226 localization, we tested the localization and contribution to aminoglycoside and stress
227 tolerance of AcrA, a protein previously identified in *E. coli* inner-membrane DRM
228 fractions often biochemically associated with FMM (37). AcrA is an efflux pump
229 involved in the transport of a wide range of substrates including aminoglycosides (48).
230 However, while an *acrA* deletion did not altered *E. coli* MIC profile to tobramycin and
231 paraquat as much as a Δ*hflC* mutant (Fig.5CD), the expression of AcrA-GFP from their
232 native chromosomal context did not lead to any distinct polar co-localization with HflC
233 in exponential or stationary phase conditions (Sup. Fig. S7).

234

235 Taken together, these results indicate that the HflKC SPFH protein complex contributes
236 to oxidative and antibiotic stress resistance.

237

238

239 **DISCUSSION**
240

241 SPFH-domain proteins have been identified in most organisms (16, 49) and extensively
242 studied in eukaryotes (3, 5, 50). By contrast, prokaryotic SPFH proteins and proteins
243 associated with functional membrane microdomains (FMMs) are much less understood.
244 This is particularly the case for Gram-negative bacteria, in which potential FMMs
245 functions are mostly inferred from studies performed in *B. subtilis* and *S. aureus*. In this
246 study, we investigated the functions and the localization determinants of *E. coli* SPFH
247 proteins. Focusing on QmcA and HflKC SPFH proteins, we used a domain deletion and
248 replacement approach and showed that most of the tested domain replacement variants
249 correctly localized to the inner membrane but failed to display WT protein localization
250 patterns. This indicates that inner-membrane localization alone is not sufficient for the
251 correct subcellular distribution of HflC and QmcA, whose localization signals might rely
252 on multiple addressing sequences spread throughout the entirety of each protein.
253 Alternatively, it has been shown that oligomerization is critical for flotillin function and
254 cluster formation (51), a process that is likely to be abolished in the domain deletion
255 constructs, potentially explaining some of the observed localization defects.
256

257 QmcA and HflKC SPFH proteins display different localization patterns and could be part
258 of different FMMs, potentially using different localization signals. The punctate
259 localization pattern displayed by QmcA-GFP fusion was also observed in the case of *E.*
260 *coli* YqiK expressed from plasmid and other Gram-positive bacteria flotillin
261 homologues(15, 16, 18, 52, 53). Interestingly, *B. subtilis*, *B. anthracis* and *S. aureus*
262 flotillin genes are physically associated with a gene encoding a NfeD protein, which could
263 contribute to protein-protein interactions within flotillin assemblies (54, 55). Consistently,
264 *E. coli qmcA* gene is located upstream of the NfeD-like *ybbJ* gene, like NfeD-like *yqiJ*
265 gene is located upstream of *yqiK* (see Supplementary Figure S1). This further supports
266 the notion that QmcA and YqiK could be considered as *E. coli bona fide* flotillins. By
267 contrast, the *hflKC* transcription unit is not closely associated with a *nfeD*-like gene,
268 suggesting that HflKC may not be a flotillin. However, while QmcA and YqiK have an
269 opposite orientation to HflK and HflC, they are structurally similar proteins and the four
270 *E. coli* SPFH proteins could therefore share some degrees of functionalities. The
271 topological similarity between HflK and HflC might contribute to HflKC complex

272 formation, and its interaction with FtsH protease, resulting in a large periplasmic FtsH-
273 HflKC complex localized at the cell pole (29, 30, 56-58).
274 The strong negative impact of QmcA or HflC transmembrane (TM) domain replacement
275 suggests that QmcA or HflC TM domains could recognize specific FMM membrane
276 lipids facilitating the recruitment of SPFH proteins at their proper cellular membrane
277 localization. Along with phosphatidylethanolamine and phosphatidylglycerol,
278 cardiolipins are the primary constituent components of *E. coli* membranes that
279 concentrate into cell poles and dividing septum (59-62). It was indeed observed that the
280 composition of *E. coli* membrane lipids at cell poles is altered in a *clsABC* cardiolipin
281 deficient mutant, compensated by an increased amount of phosphatidylglycerol (17, 63).
282 Several studies also reported that cardiolipin-enriched composition in membranes at cell
283 poles influences both the localization and activity of inner membrane proteins, such as
284 respiratory chain protein complexes and the osmosensory transporter ProP (41, 42, 64-
285 66). We showed here that, similarly to ProP, HflC and QmcA localization patterns are
286 affected in a *ΔclsABC* mutant, suggesting that HflKC and QmcA complexes could act as
287 scaffolds for cardiolipin-enriched FMM cargo proteins. Isoprenoid lipids such as farnesol,
288 carotenoids, and hopanoids have been proposed to be constituents of bacterial FMMs or
289 to interact with SPFH proteins and FMM-associated proteins (14). Consistently, blocking
290 the *S. aureus* carotenoid synthetic pathway by zaragozic acid leads to flotillin mis-
291 localization (15), and the inactivation of farnesol synthesis in a *B. subtilis yisP* mutant
292 impairs focal localization of the FMM-associated sensor kinase KinC (15). We showed
293 that interfering with the *E. coli idi* isoprenoid biosynthesis pathway also strongly alters
294 the localization of HflC. This further indicates that isoprenoid lipids contribute to the
295 formation or integrity of FMMs, possibly by altering isoprenoid-dependent membrane
296 fluidity, as shown in *S. aureus* and *B. subtilis* FMMs (14, 67).
297
298 Our investigation of the phenotypes displayed by an *E. coli* mutant lacking all SPFH
299 protein genes showed that the absence of HflKC leads to an increased susceptibility to
300 oxidative stress and aminoglycosides. The HflKC complex was previously shown to
301 modulate the quality control proteolytic activity of FtsH by regulating the access of
302 misfolded membrane protein products to FtsH (29, 30, 68). *E. coli* Δ*hflK* and Δ*hflC*
303 mutant strains were also shown to accumulate increased amounts of hydroxyl radical,

304 suggesting that HflK and HflC could influence tolerance to aminoglycosides and
305 oxidative stress by suppressing excessive hydroxyl radical production. Alternatively,
306 HflK and HflC could contribute to tobramycin resistance via FtsH-dependent proteolytic
307 activity (69) or favoring FMM formation and the assembly of membrane proteins and
308 lipids, such as cardiolipin, involved in the transport and movement of aminoglycosides
309 within cells and cell membranes. Consistently, several proteins associated with
310 aminoglycosides transport were actually detected in *E. coli* DRM fractions, including
311 transporters and several components of the AcrAB-TolC efflux pump (37), suggesting
312 that deletion of *hflK* or *hflC* could reduce the activity of these proteins in FMMs and
313 enhance entry of aminoglycosides. Whereas the susceptibility to aminoglycosides indeed
314 partly relies on the AcrAB-TolC efflux pump (48, 70-72), we found that lack of the AcrA
315 only moderately decreases the MIC to tobramycin, compared to a *hflKC* mutation. We
316 also showed that the alteration of the cardiolipin pathway in a Δ*clsABC* mutant altered
317 both the localization and sensitivity to tobramycin and paraquat of a HflC-GFP fusion.
318 This suggests that cardiolipin could be required for the correct localization of HflKC to
319 FMMs at cell poles. By contrast, although an *idi* isoprenoid pathway mutant mildly affects
320 HflC localization, it does not show altered sensitivity. This may be due to an uncomplete
321 inactivation of the pathway since lycopene production in a Δ*idi* mutant is reduced by 1/3
322 but not totally abolished, due to the fact that the idi protein is a reversible isomerase. (46).
323

324 In conclusion, the present study provides new insights into the functions of *E. coli* SPFH
325 proteins and some of their interacting partners and further experiments will be needed to
326 fully uncover the roles played by this intriguing family of membrane proteins in Gram-
327 negative bacteria.

328

329 **MATERIALS & METHODS**

330

331 **Bacterial strains and growth conditions**

332 Bacterial strains and plasmids used in this study are described in Sup. Table S2, and
333 further explained in Sup. Fig. S1 and Figure 3. Unless stated otherwise, all experiments
334 were performed in lysogeny broth (LB) or M63B1 minimal medium supplemented with
335 0.4% glucose (M63B1.G) at 37 °C. Antibiotics were used as follows: kanamycin (50
336 µg/mL); chloramphenicol (25 µg/mL); ampicillin (100 µg/mL); and zeocin (50 µg/mL).
337 All compounds were purchased from Sigma-Aldrich (St Louis, MO, USA) except for
338 Zeocin (InvivoGen, Santa Cruz, CA, USA).

339

340 **Mutant construction**

341 *Generation of mutants in E. coli:* Briefly, *E. coli* deletion or insertion mutants used in this
342 study originated either from the *E. coli* Keio collection of mutants (73) or were generated
343 by λ-red linear recombination using pKOBEG (Cm^R) or pKOBEGA (Amp^R) plasmids
344 (74) using primers listed in Sup. Table S3. P1vir transduction was used to transfer
345 mutations between different strains. When required, antibiotic resistance markers flanked
346 by two FRT sites were removed using the Flp recombinase (75). Plasmids used in this
347 study were constructed using an isothermal assembly method, Gibson assembly (New
348 England Biolabs, Ipswich, MA, USA) using primers listed in Sup. Table S3. The integrity
349 of all cloned fragments, mutations, and plasmids was verified by PCR with specific
350 primers and DNA sequencing

351

352 *Construction of deletion mutants*

353 Δ*yqiK*, Δ*qmcA*, Δ*hflK*, Δ*hflC*, Δ*clsA*, Δ*clsB*, Δ*clsC*, Δ*idi*, Δ*acrA*, deletions were
354 transferred into *E. coli* MG1655*strep* by P1vir phage transduction from the corresponding
355 mutants in the *E. coli* BW25113 background of the Keio collection (73). The associated
356 kanamycin marker was then removed using the Flp recombinase expressed from the
357 plasmid pCP20 (75). (Details regarding the construction of all other strains used in this
358 study are presented in Sup.Table S2).

359

360 *Construction of GFP and mCherry* fusions

361 See Supplementary Methods section in Supplementary Materials
362
363 *Construction of complemented strains*
364 The *hflKC* genes were amplified from MG1655*strep* using primers listed in
365 Supplementary Table S3 and cloned at the downstream of the IPTG-inducible promoter
366 of a pZS*12 vector using the Gibson assembly to generate plasmids pZS*12-HflKC Then,
367 these plasmids were introduced into Δ*hflKC* mutants, respectively, to construct
368 complemented mutants (Sup. Table S2). A pZS*12 empty vector was also introduced into
369 wildtype and Δ*hflKC* mutants. Mutants harbouring these pZS*12 plasmids were
370 incubated and used for the below experiments in the presence of IPTG (1 mM) and
371 ampicillin.
372
373 **Epifluorescence microscopy**
374 Bacteria were incubated into 5 mL of fresh LB medium and harvested at OD_{600} 0.4 for
375 samples in exponential phase or OD_{600} 2.0 for stationary phase. After washing twice with
376 M63B1 medium, cells corresponding to 1 mL of the bacterial culture were pelleted by
377 centrifugation and resuspended into 0.1 mL of M63B1 medium for exponential samples,
378 or 1 mL of the medium for stationary samples. Ten µL aliquots of the cell suspension
379 were immobilized on glass slides previously covered with freshly made M63B1 medium
380 0.8% agarose pads. Cells were observed using a ZEISS Definite focus fluorescent
381 microscope (Carl Zeiss, Oberkochen, Germany), equipped with an oil-immersion
382 objective lens microscope (Pln-Apo 63X/1.4 oil Ph3). GFP or mCherry fluorescence was
383 exited with a ZEISS Colibri LED illumination system and the fluorescence signal was
384 detected with Zeiss FS38 HE (Carl Zeiss) or Semrock HcRed filters (Semrock, Rochester,
385 NY, USA). GFP, and mCherry fluorescence images were taken at 1000, and 2000 msec.
386 exposure, respectively. Image processing was performed using ImageJ and Adobe
387 Photoshop. For each tested mutant, the subcellular localization patterns of 150 randomly
388 selected bacteria were evaluated and the frequencies were expressed as percentiles.
389
390 **Super-resolution microscopy**
391 Bacteria were imaged using single-molecule localization microscopy and stochastic
392 optical reconstruction microscopy (SMLM-STORM), using a previously described

393 method (76). Overnight cultures were fixed with PFA 4%, permeabilized with Triton
394 0,05%, and labeled with either GFP monoclonal FluoTag®-Q — Sulfo-Cyanine 5 (Cy5),
395 or RFP monoclonal FluoTag®-Q – Cy5, which are single-domain antibodies (sdAb)
396 conjugated to Cy5. Labeling was performed at 1:250 (concentration), and washing steps
397 were carried out three times using Abbelight's SMART kit buffer. For imaging,
398 Abbelight's imaging system was used with NEO software. Abbelight's module was added
399 to an Olympus IX83 with 100x TIRF objective, N.A. 1.49. We used Hamamatsu's
400 sCMOS Flash 4 camera and a 647nm 500mW Oxxius laser, with an astigmatic lens, to
401 allow for 3D imaging of the sample (77).
402
403 **Inner membrane separation**
404 *E. coli* overnight cultures were diluted into 1 L of fresh LB medium to OD_{600} of 0.02 and
405 incubated at 37°C and 180 rpm until reaching OD_{600} 0.4. Cells were harvested and washed
406 once with 10 mM HEPES (pH 7.4) and stored at -20°C for at least 1 h. Bacteria were then
407 resuspended in 10 mL of 10 mM HEPES (pH 7.4) containing 100 µL of Benzonase (3.10^4
408 U/mL) and were passed through a FRENCH press (Thermo) at 20,000 psi. The lysate was
409 centrifugated at 15,000 *g* for 15 min at 4 °C to remove cell debris, and aliquots of the
410 suspension were stored at 4 °C as the whole extract. Then, the suspension was centrifuged
411 at 100,000 *g* for 45 min at 4 °C to separate supernatant and pellets, and aliquots of the
412 supernatant were stored at 4 °C as the cytosolic and periplasmic fractions. The pellets
413 were suspended into 600 µL of cold 10 mM HEPES (pH 7.4) and homogenized by using
414 2 mL tissue grinder (Kontes Glass, Vineland, NJ, USA). Discontinuous sucrose gradients
415 with the following composition were placed into ultracentrifugation tube: bottom to top
416 0.5 mL of 2 M sucrose, 2.0 mL of 1.5 M sucrose, and 1.0 mL of 0.8 M sucrose, and 500
417 µL of the homogenized samples were placed on the top of sucrose gradients. The
418 gradients were centrifuged at 100,000 *g* for 17.5 h at 4 °C. Subsequently, 400 µL of
419 aliquots were collected into 11 microtubes from top to bottom, and the samples were
420 proceeded to the immunodetection method, as described below.
421
422 **Immunodetection of inner membrane proteins**
423 Aliquots of samples were suspended in 4× Laemmli buffer (BioRad) with 2-
424 Mercaptoethanol (Sigma) and incubated for 5 min at 98 °C. The protein samples (10 µL

425 each) were run on 4-20 % Mini-PROTEAN TGX Stain-FreeTM precast Gels (BioRad)
426 in 1× TGX buffer and then transferred to nitrocellulose membrane using a Trans-Blot®
427 Turbo™ Transfer System (BioRad). Subsequently, the membranes were blocked using
428 blocking buffer consisting of 5% skim milk in PBS with 0.05% Tween 20 (PBST) for 2
429 h at 4 °C with agitation. The membranes were then incubated in PBST containing 1%
430 skim milk with first antibodies, polyclonal rabbit antiserum raised against ExbB and TolC
431 (kindly given by Dr. Philippe Delepelaire), GFP (Invitrogen, A6455, Thermo Fisher
432 Scientific, Indianapolis, IN, USA) and mCherry (Invitrogen, PA5-34974) at 1:20,000
433 overnight at 4 °C with agitation. The membranes were washed in PBST and incubated in
434 PBST containing 1% skim milk with a secondary antibody, anti-rabbit IgG conjugated
435 with horseradish peroxidase (Cell signaling, 7074S), at 1:10,000 for 2 h at 25 °C with
436 agitation. After washing the excess secondary antibody, specific bands were visualized
437 using the ECL prime detection method (GE Healthcare) and imaged with an imaging
438 system, iBright^{TM} CL1500 (Invitrogen).
439
440 **Microbial growth phenotypic analysis**
441 A high-throughput analysis for microbial growth phenotypes using a colorimetric reaction,
442 Phenotype MicroArrays (Biolog Inc., Hayward, CA, USA), was performed in accordance
443 with the manufacturer's protocol. Briefly, several colonies of *E. coli* grown on LB agar
444 were transferred in 10 mL of a mixture of Biolog IF-0a media (BioLog) and sterilized
445 water into a sterile capped test tube. The suspension was mixed gently, and the turbidity
446 was adjusted to achieve the appropriate transmittance using the Biolog turbidimeter
447 (BioLog). The cell suspension was diluted with the IF-0a plus dye mix, as mentioned in
448 the manufacturer's protocol. 100 μL of the mixture suspension was inoculated into PM
449 plates 1-3 and 9-20 and incubated for 72 h at 37 °C. The absorbance of each well was
450 taken every 15 min. The OmniLog software (BioLog) was used to view and edit data, to
451 compare data lists, and to generate reports.
452
453 **Monitoring of bacterial growth**
454 An overnight culture of *E. coli* was diluted into fresh LB and M63B1 supplemented with
455 0.4% glucose medium to OD_{600} of 0.05, and 200 μL aliquots were cultured in the presence
456 or absence of paraquat (Methyl viologen dichloride hydrate, Sigma-Aldrich) in 96-well

457 microplates at 37 °C for 24 h with shaking. The absorbance of each culture at 600 nm was
458 measured every 15 min for 24 h using a microplate reader (Tecan Infinite, Mannedorf,
459 Switzerland).
460
461 **Susceptibility of *E. coli* against Tobramycin and Paraquat**
462 The broth microdilution method was used to determine the MIC (minimum inhibitory
463 concentration) values of Tobramycin (Sigma-Aldrich) and Paraquat (Sigma-Aldrich) in
464 96-well microtiter plates. Briefly, 100 μL of LB medium was distributed into each well
465 of the microtiter plates. Tobramycin was 2-fold serially diluted in each well. Five μL of
466 approximately 1×10^7 CFU/mL of *E. coli* was inoculated into each well, and the plates
467 were incubated at 37°C for 24 h. The lowest concentration that visibly inhibited bacterial
468 growth was defined as the MIC. All strains were evaluated in biological and technical
469 triplicates.
470 The spot assay was performed to evaluate the susceptibility of *E. coli* against
471 paraquat. Briefly, an overnight culture of *E. coli* was diluted into fresh LB medium to
472 OD_{600} of 0.05. Ten μL of the diluted culture was spotted on LB plates containing either
473 no or 100 μM paraquat. The plates were incubated at 37°C for 24 h, and the photographs
474 were taken. All strains were evaluated in triplicate.
475
476 **Statistical analysis**
477 Data analysis was performed using GraphPad Prism 9.5 software (GraphPad, La Jolla,
478 CA, USA). All data are expressed as mean (± standard deviation, SD) in figures.
479 Statistical analysis was performed using unpaired non-parametric Mann-Whitney test.
480 Differences were considered statistically significant for P values of <0.05.

ACKNOWLEDGMENTS

We thank Philippe Delepelaire for insightful comments and material support. We thank Uwe Sauer and Philip Warmer for initial assessment of lipid composition of some of the strains used in this study. We are grateful to Eva Wolrab and Sven van Teeffelen for their initial interest in the project and for providing the strains for msfGFP and mCherry constructions. This work was supported by EU Horizon 2020 Rafts4Biotech grant 720776 (to JMG, DL, AKW, YY, AR, UV and MS), the French government's Investissement d'Avenir Program, Laboratoire d'Excellence "Integrative Biology of Emerging Infectious Diseases" (grant n°ANR-10-LABX-62-IBEID) and the *Fondation pour la Recherche Médicale* (grant no. DEQ20180339185). This work benefited from the facilities and expertise of Add Photonic BioImaging platform (UTechS PBI, Institut Pasteur). A.K.W. was supported by a Pasteur-Roux-Cantarini postdoctoral and a grant from the Philippe Foundation.

AUTHOR CONTRIBUTIONS:

A.K.W., Y.Y., and J.-M.G. designed the experiments. A.K.W., Y.Y., A.R., R.B.; M.S., J.B-B. performed the experiments. A.K.W., Y.Y., A.R., U.V. M.S., R.B., J.-M.B., C.B., D.L. and J.-M.G. analyzed the data. Y.Y., A.K.W. and J.-M.G. wrote the paper with significant contribution from all authors.

DATA AVAILABILITY

The data that support the findings of this study are presented in the paper and/or the Supplementary Materials. Strains and plasmids are available from the corresponding author, JMG, upon reasonable request.

COMPETING INTERESTS

The authors declare no competing financial or non-financial interests.

508 **REFERENCES**
509

510 1. Alberts B, Johnson A, Lewis J, Raff M, Roberts K, Walter P. 2002. Molecular
511 biology of the cell 6th edition ed. Garland Science., New York.
512 2. Cho W, Stahelin RV. 2005. Membrane-protein interactions in cell signaling and
513 membrane trafficking. Annu Rev Biophys Biomol Struct 34:119-51.
514 3. Simons K, Ikonen E. 1997. Functional rafts in cell membranes. Nature 387:569-
515 72.
516 4. Rajendran L, Simons K. 2005. Lipid rafts and membrane dynamics. J Cell Sci
517 118:1099-102.
518 5. Simons K, Sampaio JL. 2011. Membrane organization and lipid rafts. Cold
519 Spring Harb Perspect Biol 3:a004697.
520 6. Pike LJ. 2006. Rafts defined: a report on the Keystone Symposium on Lipid
521 Rafts and Cell Function. J Lipid Res 47:1597-8.
522 7. Sezgin E, Levental I, Mayor S, Eggeling C. 2017. The mystery of membrane
523 organization: composition, regulation and roles of lipid rafts. Nat Rev Mol Cell
524 Biol 18:361-374.
525 8. Langhorst MF, Reuter A, Stuermer CA. 2005. Scaffolding microdomains and
526 beyond: the function of reggie/flotillin proteins. Cell Mol Life Sci 62:2228-40.
527 9. Morrow IC, Parton RG. 2005. Flotillins and the PHB domain protein family:
528 rafts, worms and anaesthetics. Traffic 6:725-40.
529 10. Stuermer CA, Plattner H. 2005. The 'lipid raft' microdomain proteins reggie-1
530 and reggie-2 (flotillins) are scaffolds for protein interaction and signalling.
531 Biochem Soc Symp doi:10.1042/bss0720109:109-18.
532 11. Browman DT, Hoegg MB, Robbins SM. 2007. The SPFH domain-containing
533 proteins: more than lipid raft markers. Trends Cell Biol 17:394-402.
534 12. Zeke A, Lukács M, Lim WA, Reményi A. 2009. Scaffolds: interaction platforms
535 for cellular signalling circuits. Trends Cell Biol 19:364-74.
536 13. Zhao F, Zhang J, Liu YS, Li L, He YL. 2011. Research advances on flotillins.
537 Virol J 8:479.
538 14. Lopez D, Koch G. 2017. Exploring functional membrane microdomains in
539 bacteria: an overview. Curr Opin Microbiol 36:76-84.
540 15. Lopez D, Kolter R. 2010. Functional microdomains in bacterial membranes.
541 Genes Dev 24:1893-902.
542 16. Bramkamp M, Lopez D. 2015. Exploring the existence of lipid rafts in bacteria.
543 Microbiol Mol Biol Rev 79:81-100.
544 17. Koppelman CM, Den Blaauwen T, Duursma MC, Heeren RM, Nanninga N.
545 2001. Escherichia coli minicell membranes are enriched in cardiolipin. J
546 Bacteriol 183:6144-7.
547 18. García-Fernández E, Koch G, Wagner RM, Fekete A, Stengel ST, Schneider J,
548 Mielich-Süss B, Geibel S, Markert SM, Stigloher C, Lopez D. 2017. Membrane
549 Microdomain Disassembly Inhibits MRSA Antibiotic Resistance. Cell
550 171:1354-1367.e20.
551 19. Willdigg JR, Helmann JD. 2021. Mini Review: Bacterial Membrane
552 Composition and Its Modulation in Response to Stress. Front Mol Biosci
553 8:634438.
554 20. Dempwolff F, Möller HM, Graumann PL. 2012. Synthetic motility and cell
555 shape defects associated with deletions of flotillin/reggie paralogs in Bacillus

556 subtilis and interplay of these proteins with NfeD proteins. J Bacteriol 194:4652-
557 61.
558 21. Bach JN, Bramkamp M. 2013. Flotillins functionally organize the bacterial
559 membrane. Mol Microbiol 88:1205-17.
560 22. Schneider J, Klein T, Mielich-Süss B, Koch G, Franke C, Kuipers OP, Kovács Á
561 T, Sauer M, Lopez D. 2015. Spatio-temporal remodeling of functional
562 membrane microdomains organizes the signaling networks of a bacterium. PLoS
563 Genet 11:e1005140.
564 23. Wagner RM, Kricks L, Lopez D. 2017. Functional Membrane Microdomains
565 Organize Signaling Networks in Bacteria. J Membr Biol 250:367-378.
566 24. Donovan C, Bramkamp M. 2009. Characterization and subcellular localization
567 of a bacterial flotillin homologue. Microbiology 155:1786-1799.
568 25. Yepes A, Schneider J, Mielich B, Koch G, García-Betancur JC, Ramamurthi
569 KS, Vlamakis H, López D. 2012. The biofilm formation defect of a Bacillus
570 subtilis flotillin-defective mutant involves the protease FtsH. Mol Microbiol
571 86:457-71.
572 26. Mielich-Süss B, Schneider J, Lopez D. 2013. Overproduction of flotillin
573 influences cell differentiation and shape in Bacillus subtilis. mBio 4:e00719-13.
574 27. Schneider J, Mielich-Süss B, Böhme R, Lopez D. 2015. In vivo characterization
575 of the scaffold activity of flotillin on the membrane kinase KinC of Bacillus
576 subtilis. Microbiology 161:1871-1887.
577 28. Hinderhofer M, Walker CA, Friemel A, Stuermer CA, Möller HM, Reuter A.
578 2009. Evolution of prokaryotic SPFH proteins. BMC Evol Biol 9:10.
579 29. Kihara A, Akiyama Y, Ito K. 1996. A protease complex in the Escherichia coli
580 plasma membrane: HflKC (HflA) forms a complex with FtsH (HflB), regulating
581 its proteolytic activity against SecY. Embo j 15:6122-31.
582 30. Saikawa N, Akiyama Y, Ito K. 2004. FtsH exists as an exceptionally large
583 complex containing HflKC in the plasma membrane of Escherichia coli. J Struct
584 Biol 146:123-9.
585 31. Chiba S, Ito K, Akiyama Y. 2006. The Escherichia coli plasma membrane
586 contains two PHB (prohibitin homology) domain protein complexes of opposite
587 orientations. Mol Microbiol 60:448-57.
588 32. Ma C, Wang C, Luo D, Yan L, Yang W, Li N, Gao N. 2022. Structural insights
589 into the membrane microdomain organization by SPFH family proteins. Cell
590 Res 32:176-189.
591 33. Brown DA, Rose JK. 1992. Sorting of GPI-anchored proteins to glycolipid-
592 enriched membrane subdomains during transport to the apical cell surface. Cell
593 68:533-44.
594 34. Schroeder R, London E, Brown D. 1994. Interactions between saturated acyl
595 chains confer detergent resistance on lipids and glycosylphosphatidylinositol
596 (GPI)-anchored proteins: GPI-anchored proteins in liposomes and cells show
597 similar behavior. Proc Natl Acad Sci U S A 91:12130-4.
598 35. Lichtenberg D, Goñi FM, Heerklotz H. 2005. Detergent-resistant membranes
599 should not be identified with membrane rafts. Trends Biochem Sci 30:430-6.
600 36. Brown DA. 2006. Lipid rafts, detergent-resistant membranes, and raft targeting
601 signals. Physiology (Bethesda) 21:430-9.
602 37. Guzmán-Flores JE, Steinemann-Hernández L, González de la Vara LE,
603 Gavilanes-Ruiz M, Romeo T, Alvarez AF, Georgellis D. 2019. Proteomic

604 analysis of Escherichia coli detergent-resistant membranes (DRM). PLoS One
605 14:e0223794.
606 38. Guzman-Flores JE, Alvarez AF, Poggio S, Gavilanes-Ruiz M, Georgellis D.
607 2017. Isolation of detergent-resistant membranes (DRMs) from Escherichia coli.
608 Anal Biochem 518:1-8.
609 39. Ito K, Akiyama Y. 2005. Cellular functions, mechanism of action, and
610 regulation of FtsH protease. Annu Rev Microbiol 59:211-31.
611 40. Padilla-Vaca F, Vargas-Maya NI, Elizarrarás-Vargas NU, Rangel-Serrano Á,
612 Cardoso-Reyes LR, Razo-Soria T, Membrillo-Hernández J, Franco B. 2019.
613 Flotillin homologue is involved in the swimming behavior of Escherichia coli.
614 Arch Microbiol 201:999-1008.
615 41. Romantsov T, Helbig S, Culham DE, Gill C, Stalker L, Wood JM. 2007.
616 Cardiolipin promotes polar localization of osmosensory transporter ProP in
617 Escherichia coli. Mol Microbiol 64:1455-65.
618 42. Mileykovskaya E, Dowhan W. 2009. Cardiolipin membrane domains in
619 prokaryotes and eukaryotes. Biochim Biophys Acta 1788:2084-91.
620 43. Feng X, Hu Y, Zheng Y, Zhu W, Li K, Huang CH, Ko TP, Ren F, Chan HC,
621 Nega M, Bogue S, López D, Kolter R, Götz F, Guo RT, Oldfield E. 2014.
622 Structural and functional analysis of Bacillus subtilis YisP reveals a role of its
623 product in biofilm production. Chem Biol 21:1557-63.
624 44. Zielińska A, Savietto A, de Sousa Borges A, Martinez D, Berbon M, Roelofsen
625 JR, Hartman AM, de Boer R, van der Klei IJ, Hirsch AKH, Habenstein B,
626 Bramkamp M, Scheffers D-J. 2020. Flotillin mediated membrane fluidity
627 controls peptidoglycan synthesis and MreB movement. bioRxiv
628 doi:10.1101/736819:736819.
629 45. Nishijima S, Asami Y, Uetake N, Yamagoe S, Ohta A, Shibuya I. 1988.
630 Disruption of the Escherichia coli cls gene responsible for cardiolipin synthesis.
631 J Bacteriol 170:775-80.
632 46. Hemmi H, Ohnuma S, Nagaoka K, Nishino T. 1998. Identification of genes
633 affecting lycopene formation in Escherichia coli transformed with carotenoid
634 biosynthetic genes: candidates for early genes in isoprenoid biosynthesis. J
635 Biochem 123:1088-96.
636 47. Hahn FM, Hurlburt AP, Poulter CD. 1999. Escherichia coli open reading frame
637 696 is idi, a nonessential gene encoding isopentenyl diphosphate isomerase. J
638 Bacteriol 181:4499-504.
639 48. Aires JR, Nikaido H. 2005. Aminoglycosides are captured from both periplasm
640 and cytoplasm by the AcrD multidrug efflux transporter of Escherichia coli. J
641 Bacteriol 187:1923-9.
642 49. Tavernarakis N, Driscoll M, Kyrpides NC. 1999. The SPFH domain: implicated
643 in regulating targeted protein turnover in stomatins and other membrane-
644 associated proteins. Trends Biochem Sci 24:425-7.
645 50. Morrow IC, Rea S, Martin S, Prior IA, Prohaska R, Hancock JF, James DE,
646 Parton RG. 2002. Flotillin-1/reggie-2 traffics to surface raft domains via a novel
647 golgi-independent pathway. Identification of a novel membrane targeting
648 domain and a role for palmitoylation. J Biol Chem 277:48834-41.
649 51. Bach JN, Bramkamp M. 2015. Dissecting the molecular properties of
650 prokaryotic flotillins. PLoS One 10:e0116750.

651 52. Dempwolff F, Schmidt FK, Hervás AB, Stroh A, Rösch TC, Riese CN, Dersch
652 S, Heimerl T, Lucena D, Hülsbusch N, Stuermer CA, Takeshita N, Fischer R,
653 Eckhardt B, Graumann PL. 2016. Super Resolution Fluorescence Microscopy
654 and Tracking of Bacterial Flotillin (Reggie) Paralogs Provide Evidence for
655 Defined-Sized Protein Microdomains within the Bacterial Membrane but
656 Absence of Clusters Containing Detergent-Resistant Proteins. PLoS Genet
657 12:e1006116.
658 53. Somani VK, Aggarwal S, Singh D, Prasad T, Bhatnagar R. 2016. Identification
659 of Novel Raft Marker Protein, FlotP in Bacillus anthracis. Front Microbiol
660 7:169.
661 54. Dempwolff F, Wischhusen HM, Specht M, Graumann PL. 2012. The deletion of
662 bacterial dynamin and flotillin genes results in pleiotrophic effects on cell
663 division, cell growth and in cell shape maintenance. BMC Microbiol 12:298.
664 55. Yokoyama H, Matsui I. 2020. The lipid raft markers stomatin, prohibitin,
665 flotillin, and HflK/C (SPFH)-domain proteins form an operon with NfeD
666 proteins and function with apolar polyisoprenoid lipids. Crit Rev Microbiol
667 46:38-48.
668 56. Kihara A, Ito K. 1998. Translocation, folding, and stability of the HflKC
669 complex with signal anchor topogenic sequences. J Biol Chem 273:29770-5.
670 57. Edgar R, Rokney A, Feeney M, Semsey S, Kessel M, Goldberg MB, Adhya S,
671 Oppenheim AB. 2008. Bacteriophage infection is targeted to cellular poles. Mol
672 Microbiol 68:1107-16.
673 58. Bandyopadhyay K, Parua PK, Datta AB, Parrack P. 2010. Escherichia coli HflK
674 and HflC can individually inhibit the HflB (FtsH)-mediated proteolysis of
675 lambdaCII in vitro. Arch Biochem Biophys 501:239-43.
676 59. Raetz CR, Dowhan W. 1990. Biosynthesis and function of phospholipids in
677 Escherichia coli. J Biol Chem 265:1235-8.
678 60. Lin TY, Weibel DB. 2016. Organization and function of anionic phospholipids
679 in bacteria. Appl Microbiol Biotechnol 100:4255-67.
680 61. Sohlenkamp C, Geiger O. 2016. Bacterial membrane lipids: diversity in
681 structures and pathways. FEMS Microbiol Rev 40:133-59.
682 62. El Khoury M, Swain J, Sautrey G, Zimmermann L, Van Der Smissen P, Décout
683 JL, Mingeot-Leclercq MP. 2017. Targeting Bacterial Cardiolipin Enriched
684 Microdomains: An Antimicrobial Strategy Used by Amphiphilic
685 Aminoglycoside Antibiotics. Sci Rep 7:10697.
686 63. Oliver PM, Crooks JA, Leidl M, Yoon EJ, Saghatelian A, Weibel DB. 2014.
687 Localization of anionic phospholipids in Escherichia coli cells. J Bacteriol
688 196:3386-98.
689 64. Romantsov T, Stalker L, Culham DE, Wood JM. 2008. Cardiolipin controls the
690 osmotic stress response and the subcellular location of transporter ProP in
691 Escherichia coli. J Biol Chem 283:12314-23.
692 65. Arias-Cartin R, Grimaldi S, Arnoux P, Guigliarelli B, Magalon A. 2012.
693 Cardiolipin binding in bacterial respiratory complexes: structural and functional
694 implications. Biochim Biophys Acta 1817:1937-49.
695 66. Romantsov T, Gonzalez K, Sahtout N, Culham DE, Coumoundouros C, Garner
696 J, Kerr CH, Chang L, Turner RJ, Wood JM. 2018. Cardiolipin synthase A
697 colocalizes with cardiolipin and osmosensing transporter ProP at the poles of
698 Escherichia coli cells. Mol Microbiol 107:623-638.

67. van Tilburg AY, Warmer P, van Heel AJ, Sauer U, Kuipers OP. 2022. Membrane composition and organization of Bacillus subtilis 168 and its genome-reduced derivative miniBacillus PG10. Microb Biotechnol 15:1633-1651.
68. Akiyama Y. 2009. Quality control of cytoplasmic membrane proteins in Escherichia coli. J Biochem 146:449-54.
69. Hinz A, Lee S, Jacoby K, Manoil C. 2011. Membrane proteases and aminoglycoside antibiotic resistance. J Bacteriol 193:4790-7.
70. Venter H, Mowla R, Ohene-Agyei T, Ma S. 2015. RND-type drug efflux pumps from Gram-negative bacteria: molecular mechanism and inhibition. Front Microbiol 6:377.
71. Nikaido E, Shirosaka I, Yamaguchi A, Nishino K. 2011. Regulation of the AcrAB multidrug efflux pump in Salmonella enterica serovar Typhimurium in response to indole and paraquat. Microbiology 157:648-655.
72. Garneau-Tsodikova S, Labby KJ. 2016. Mechanisms of Resistance to Aminoglycoside Antibiotics: Overview and Perspectives. Medchemcomm 7:11-27.
73. Baba T, Ara T, Hasegawa M, Takai Y, Okumura Y, Baba M, Datsenko KA, Tomita M, Wanner BL, Mori H. 2006. Construction of Escherichia coli K-12 in-frame, single-gene knockout mutants: the Keio collection. Mol Syst Biol 2:2006.0008.
74. Chaveroche MK, Ghigo JM, d'Enfert C. 2000. A rapid method for efficient gene replacement in the filamentous fungus Aspergillus nidulans. Nucleic Acids Res 28:E97.
75. Cherepanov PP, Wackernagel W. 1995. Gene disruption in Escherichia coli: TcR and KmR cassettes with the option of Flp-catalyzed excision of the antibiotic-resistance determinant. Gene 158:9-14.
76. Boudjemaa R, Cabriel C, Dubois-Brissonnet F, Bourg N, Dupuis G, Gruss A, Leveque-Fort S, Briandet R, Fontaine-Aupart MP, Steenkeste K. 2018. Impact of Bacterial Membrane Fatty Acid Composition on the Failure of Daptomycin To Kill Staphylococcus aureus. Antimicrob Agents Chemother 62.
77. Cabriel C, Bourg N, Dupuis G, Leveque-Fort S. 2018. Aberration-accounting calibration for 3D single-molecule localization microscopy. Opt Lett 43:174-177.

734 **FIGURES**

735

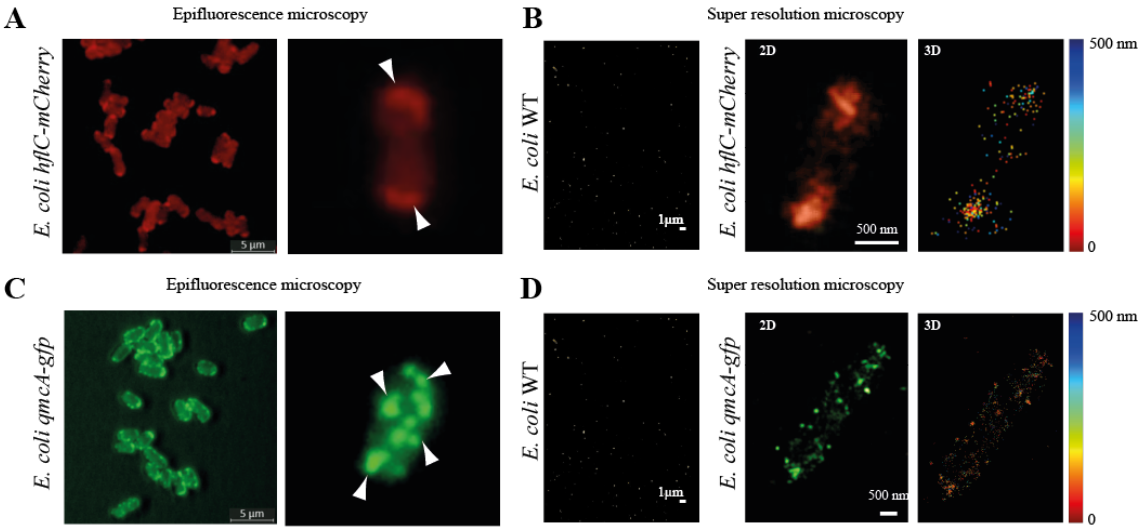

736

737 **Figure 1. Cell localization patterns of HflC and QmcA. A** and **C**: Epifluorescence
738 microscopy of cells expressing HflC-mCherry (A) or QmcA-GFP (C). Arrowheads
739 indicate polar or punctate localization foci. **B** and **D**: Super-resolution microscopy of cells
740 expressing HflC-mCherry (B) or QmcA-GFP (D). *Left panels*: lack of subcellular
741 localization in WT cells. *Center panels*: 3D images-artificial colors (red for HflC-
742 mCherry, green for QmcA-gfp). *Right panels*: 3D localization of HflC-mCherry and
743 QmcA-GFP, with colors corresponding to depth location along the Z axis, 0-500 nm, with
744 0 nm expressed in red, and 500 nm expressed in deep blue. Scales are indicated as white
745 bars.

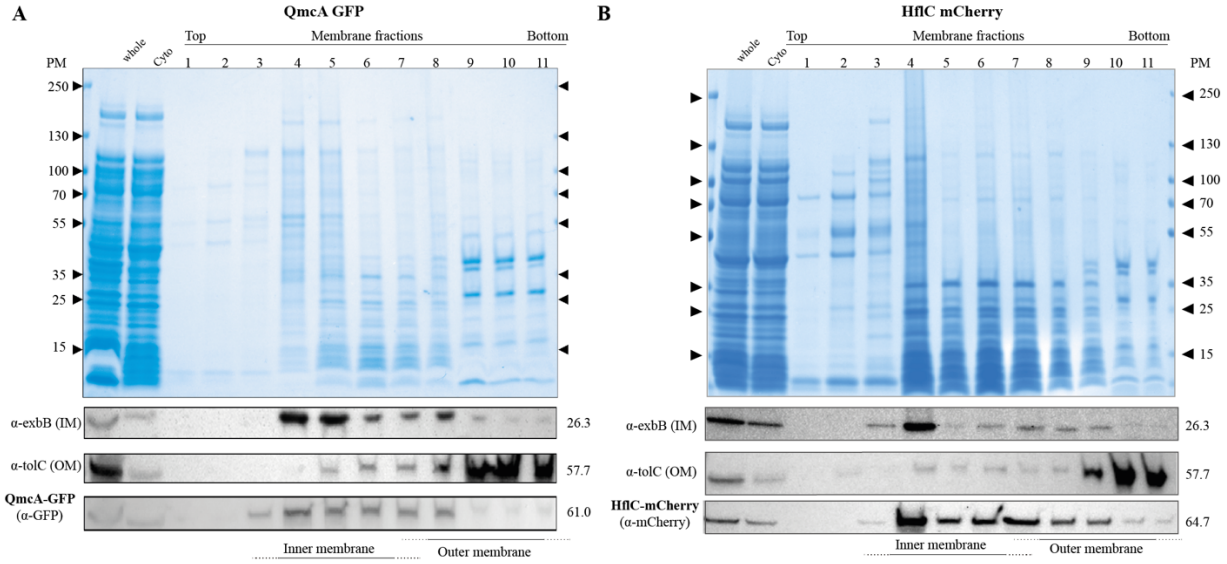

Figure 2. QmcA and HflC localize to the inner membrane. SDS-PAGE and immunodetection analyses of whole-cell extracts, cytosolic fractions, and inner (IM) or outer membrane (OM) fractions prepared from cells expressing QmcA-GFP (**A**) and HflC-mCherry (**B**). Anti-GFP and anti-mCherry antibodies were used to detect the presence of QmcA-GFP and HflC-mCherry, respectively. An anti-ExbB antibody were used to detect the inner membrane- (IM) marker ExbB and anti-TolC antibodies to detect the outer membrane- (OM) marker TolC.

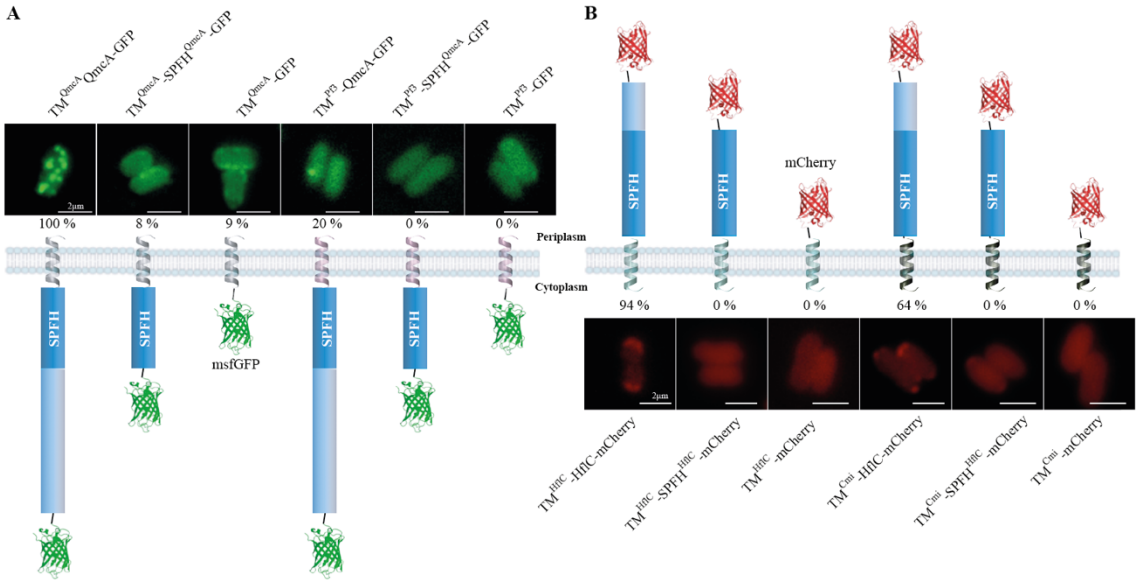

Figure 3. The localization pattern and membrane topology of full-length, domain swapped or truncated versions of QmcA and HflC. (**A**) GFP fusion derivatives of QmcA and (**B**) mCherry fusion derivatives of HflC. The representative images are shown in each strain with the frequencies of cells showing punctate (**A**) or polar localization (**B**). In membrane topology, helical structures represent transmembrane (TM) domains; silver, native TM domain of QmcA; pink, Pf3 domain; green, native TM domain of HflC; black, Cmi domain. Scale bars are 2 μm.

765
766
767

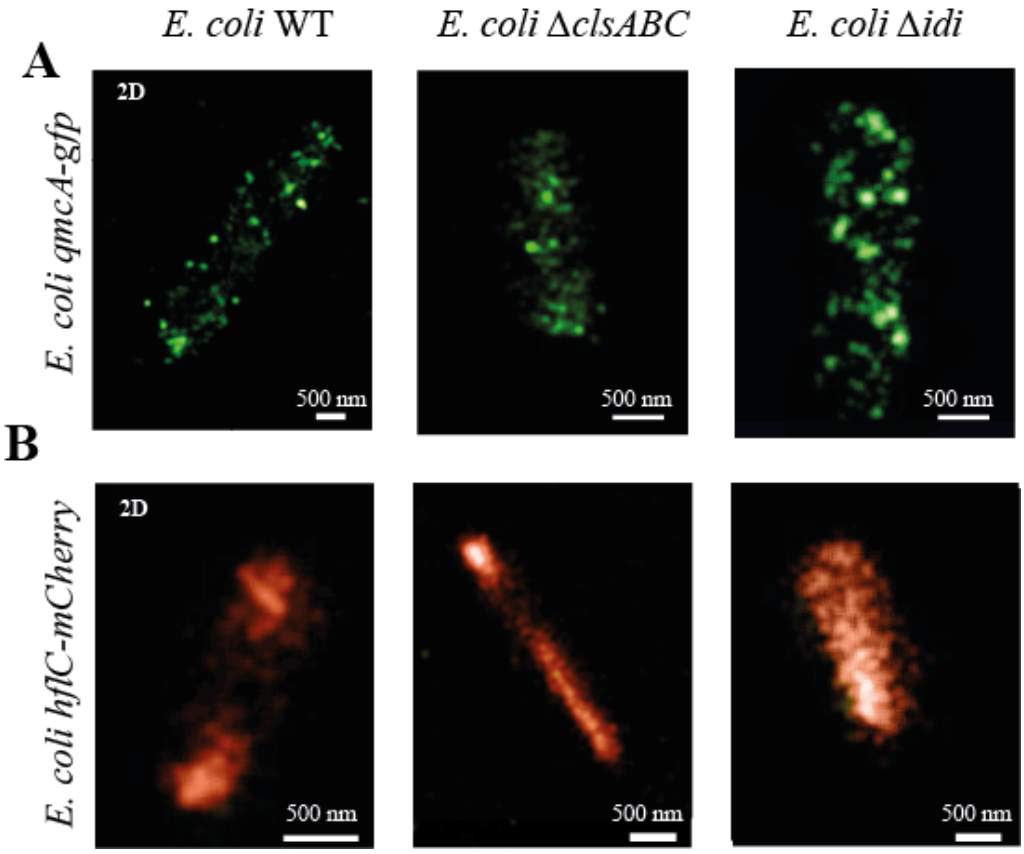

768

769 **Figure 4. Alteration of QmcA and HflC cell localization in *E. coli* cardiolipin and**
770 **isoprenoid pathway mutants.** Two-dimensional super-resolution microscopy images of
771 WT, Δ*clsABC*, and Δ*idi* strains expressing QmcA-GFP (**A**) and HflC-mCherry (**B**) in
772 stationary phase.

773
774
775

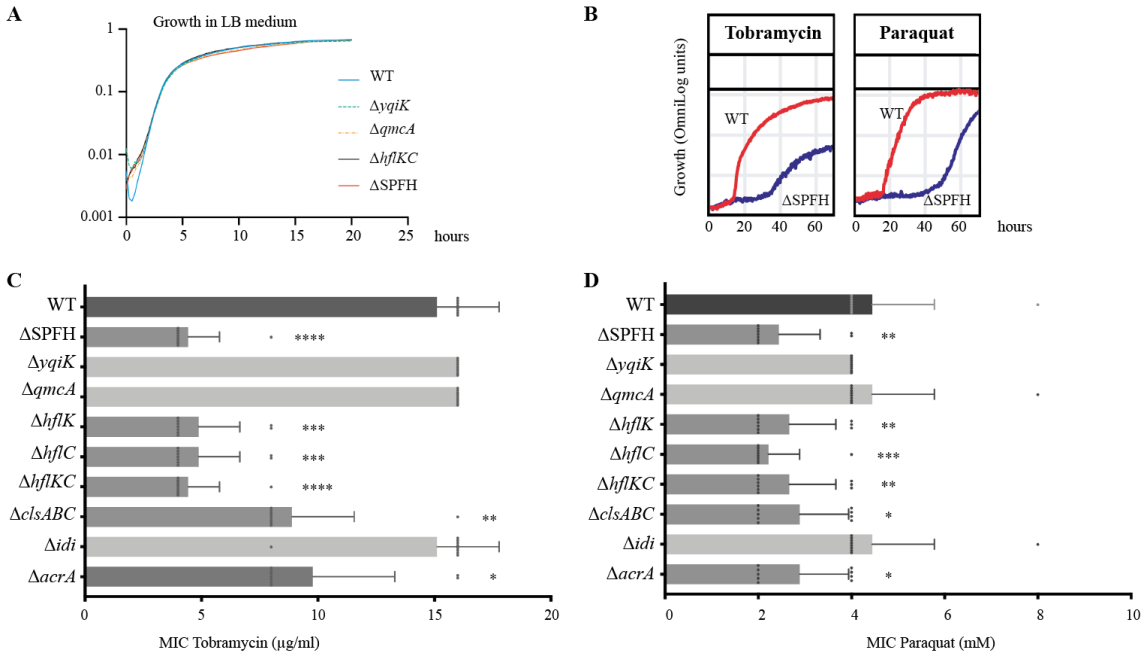

Figure 5. Phenotypic analysis of *E. coli* SPFH mutants. **A**: Bacterial growth curve of WT and SPFH gene deletion mutants in LB medium. **B**: Biolog bacterial growth curve of WT and ΔSPFH in the presence of tobramycin and paraquat. **C**: Minimum inhibitory concentration (MIC) for tobramycin of *E. coli* WT and indicated mutants. **D**: Minimum inhibitory concentration (MIC) for paraquat of *E. coli* WT and indicated mutants. *$p < 0.05$, **$p < 0.01$, ***$p < 0.001$, ****$p < 0.0001$compared with WT.